Main Manuscript for

Decoupling liquid-liquid phase separation and opalescence from stress-induced aggregation in therapeutic mAb formulations

Inna Brakti[a,b,1], Samuel Lenton[a,1], Hannes Ausserwöger[c], Rob Scrutton[c], Nikolai Lorenzen[d], Martin Nors Pedersen[b], Jesper Søndergaard Marino[e], Fátima Herranz-Trillo[f], Ann E. Terry[f], Tuomas P. J. Knowles[c], Minna Grønning Jensen[b], Vito Foderà[a]

[a]Department of Pharmacy, University of Copenhagen, Copenhagen, Denmark 2100, [b]Biophysical Analysis, CMC Analytical Support, Novo Nordisk A/S, Måløv, Denmark 2760, [c]Yusuf Hamied Department of Chemistry, Centre for Misfolding Diseases, University of Cambridge, Cambridge, United Kingdom CB2 1EW, [d]Biophysics and Injectable Formulation, Global Research Technologies, Novo Nordisk A/S, Måløv, Denmark 2760, [e]Process Optimisation, Digital Science and Innovation, Novo Nordisk A/S, Måløv, Denmark 2760,[f]MAX IV Laboratory, Lund University, Fotongatan 2, 224 84 Lund, Sweden

* Vito Foderà

Address: Department of Pharmacy, University of Copenhagen, Copenhagen, Denmark 2100

Phone: +4535336131

Email: vito.fodera@sund.ku.dk

*Minna Grønning Jensen

Address: Biophysical Analysis, CMC Analytical Support, Novo Nordisk A/S, Måløv, Denmark 2760

Phone: +4530753421

Email: mgqj@novonordisk.com

Author Contributions :

I.B: Conceptualization, Project Administration, Investigation, Visualization, Writing - Original Draft, Formal analysis, **S.L:** Conceptualization, Investigation, Visualization, Writing - Original Draft, Formal analysis, **H.A:** Investigation, Writing - Review & Editing, Formal analysis, **R.S:** Investigation, Writing - Review & Editing, Formal analysis, **M.N.P:** Supervision, **J.S.M:** Supervision, **N.L:** Writing - Review & Editing, **F.H.T:** Resources, **A.E.T:** Resources, Writing - Review & Editing,**T.P.J.K:** Resources, **M.G.J:** Conceptualization, Supervision, Project administration, Resources, Writing - Review & Editing, Funding acquisition, **V.F:** Conceptualization, Supervision, Project administration, Resources, Writing - Review & Editing, Funding acquisition

Competing Interest Statement: N.L, M.N, J.S.M and M.G.J are employees of Novo Nordisk A/S.

Classification: Biological Sciences, Biochemistry

Keywords: antibody development, formulation, liquid-liquid phase separation, opalescence, aggregation

This PDF file includes:

Main Text
Figures 1 to 4

Abstract

Liquid-liquid phase separation (LLPS) and high opalescence resulting from attractive interactions in the absence of large-scale self-association are commonly encountered in liquid monoclonal antibody (mAb) formulations and often associated with aggregation. Here, we evaluated the formulation dependent self-assembly behavior of a therapeutic mAb (termed mAb1) and provide a link to physical stability after applied stress. Using a combinatorial microdroplet platform to delineate the phase space of mAb1, we highlight its unusual solution properties. Specifically, mAb1 undergoes LLPS in a narrow window of low NaCl concentrations, in a formulation relevant design space, at room temperature (RT), without crowding agents and more than one pH unit lower than its isoelectric point. Using time-resolved small-angle X-ray scattering, we measured the attractive interactions underpinning LLPS to be on the sub second timescale and leading to the formation of small clusters, which altogether could be rapidly inhibited by L-arginine HCl. The elevated opalescence of mAb1 solutions extended beyond the LLPS regime, where a highly similar interaction fingerprint to the LLPS condition was observed but no microscopic association was detected. This suggests that LLPS and opalescence differ in the distribution of interactions within their networks, dictating their ability to form long-range assemblies (phase-separated droplets) or not. Finally, our physical stability assessment highlights that mAb1 LLPS and molecular assemblies giving rise to high opalescence both resist stirring stress and that the observed aggregation is uncorrelated with ionic strength at our selected timescale. This observation challenges an unequivocal relationship between LLPS/opalescence and reduced physical stability of mAb solutions.

Significance Statement

The development of formulations maximizing the stability of therapeutic monoclonal antibodies is a crucial part of their successful development. However, their proclivity for self-association often results in increased opalescence, which has been shown to indicate a propensity for liquid-liquid phase separation (LLPS), involving the de-mixing of solutions into two phases with different concentrations of solute. Both phenomena are commonly tied to a high propensity for aggregation. However, given the paucity of experimental studies, evidence for a general correlation between these solution properties and aggregation remains scant. In this work, we decouple stress-induced aggregation from LLPS and high opalescence without large-scale self-association through the fundamental study of these phenomena and solution integrity after applied stress.

Introduction

Since the approval in 1986 by the US Food and Drug Administration of the first monoclonal antibody (mAb) as a novel drug modality to reduce kidney transplant rejection in humans (Muromonab-CD3/), their commercial success of has been continuously expanding, with 100

unique mAb products approved as of 2021 for the treatment of a variety of medical conditions (1–4). Key factors for the success of mAbs as therapeutics include the established and versatile possibilities for antibody discovery and engineering allowing development of fine-tuned binding affinities for desired targets (1, 5). Moreover, the interaction between the fragment crystallizable region of mAbs with the neonatal Fc receptor grants them a prolonged plasma half-life, rendering less frequent administration possible (2). Therapeutic mAbs are usually administered parenterally by intravenous infusion or subcutaneous (SC) injection. For chronic disease management, the latter approach is favored, as it improves patient adherence by providing a less intrusive delivery method and the ease of self-administration at home.(6–9). However, due to their large size and often limited potency, mAbs are routinely formulated at concentrations exceeding 100 mg/mL, to deliver an effective dose at the small injection volumes imposed by the SC route (1-1.5 mL) (9, 10). In these crowded regimes, the probability of collisions between mAb molecules increases and, if these interactions are more favorable than interactions with the surrounding solvent, they can result in the formation of higher-order protein networks. This process can trigger various outcomes as curated in (11), such as the formation of reversible oligomers (clusters) that can lead to macroscopic effects including high solution viscosity (6, 12, 13), high opalescence (term often used interchangeably with turbidity) (14) and liquid-liquid phase separation (LLPS) (15, 16) or the formation of larger soluble/insoluble aggregates (17).

Opalescence is commonly observed in mAb solution and is a light scattering phenomenon that can arise from different phenomena such as net attractive interactions between molecules without association into higher order species (18), particulate matter or concentration fluctuations in solution (19, 20). LLPS is an example of the latter and occurs when solutes spontaneously associate through weak but multiple, synergistic and noncovalent interactions in solution, often mediated by surface patches of high local charge density of hydrophobicity (20, 21). This process is associated with an increased opalescent appearance as a result of the solution separating into two distinct phases: a highly concentrated, dense phase and a less concentrated, “dilute” phase (21, 22). Factors such as ionic strength modulation through the addition of salts as well as the salt type and concentration have been reported to influence mAb LLPS (23). Additional factors include the proximity of the formulation pH to the isoelectric point (pI) of the mAbs (23–27), incubation at refrigerated temperatures (≈ 4°C) and below (23, 25, 28–32), the presence of crowding agents (33), nonspecific interactions with ligands (21) and binding to smaller ionic additives (24, 34). Protein LLPS in aqueous solutions has been studied for decades (22). However, since a seminal paper from 2009 demonstrating the generation of biomolecular condensates *in vivo* through phase separation and their importance in orchestrating cellular processes, reports of protein systems exhibiting LLPS have multiplied (35).

In a drug development context opalescence above a defined threshold is often avoided in mAb solutions as it is commonly flagged as a precursor for LLPS (7) and, by extension, aggregation: two detrimental phenomena for the development of reproducible and high-quality therapeutic products. LLPS is a development concern for two reasons (1) the delicate formation and dissociation of LLPS based on changes in temperature, excipients, proteins concentration and incubation time makes it very difficult to develop proper control strategies during a product’s shelf-life and (2) it has been linked to aggregation of some protein systems (7, 28, 35). The large majority of reported LLPS-related aggregation concerns disordered protein systems (36, 37). This was recently corroborated by Linsemeier et al. (38), who observed that the surface of hnRNPA1 droplets could serve as nucleation points for fibril formation. Another study by Soumik et.al (39) revealed that ageing of phase-separated droplets accelerated the aggregation kinetics of α-synuclein. Interestingly, while droplet interfaces have been demonstrated to spearhead the aggregation fof several proteins, more recent reports also point toward a shielding role of the droplet interior, emphasizing the double-edged nature of this phenomenon (40, 41). Concerning mAbs, Pantuso et al. hypothesized that LLPS-induced partial unfolding of the Anti-CD20 mAb promoted crystal growth along the droplet surface (42). On the other hand, Bramham et al. observed that the structural integrity of the COE3 mAb was conserved upon LLPS formation and

no changes in the aggregation profile were detected after storage at refrigerated conditions (4°C) after 28 days (43). Hence, a direct experimental link between mAb LLPS and aggregation has to our knowledge not been established under formulation relevant conditions.

In this work, we aim to study the connection between LLPS and opalescence, as well as their effect on aggregation upon physical stress using a model therapeutic mAb, termed mAb1 here. Using a combination of droplet microfluidics, light scattering, and imaging techniques, we show that low NaCl concentrations induce LLPS of mAb1 above 30 mg/ml in a minimal formulation. The LLPS phase space is flanked by well-mixed states of differing opalescence levels, representing a case of mAb reentrant-like phase transition behavior. Time-resolved small-angle X-ray scattering (TR-SAXS) reveal that the interactions leading to LLPS are formed extremely rapidly (sub second timescale) and can be inhibited by adding L-arginine HCl. We further report that mAb1 LLPS and opalescence without large-scale self-association, which can be indistinguishable visibly and in light scattering properties, are both driven by attractive interactions and argue that differences in their colloidal interaction landscapes result in the observed different microstructures being formed in each case. Finally, we evaluated whether LLPS/opalescence increased aggregation, by subjecting selected formulations to contact magnetic stirring. The observed aggregation is independent of the ionic strength and the presence of LLPS/opalescence. This suggests the presence of two decoupled self-assembly mechanisms: one NaCl-dependent pathway and a stress-induced pathway independent of ionic strength. The former is characterized by LLPS at low salt followed by a reentrant phase transition to a highly opalescent, droplet-free state in proximity to the phase border, after which interactions become gradually more repulsive as the ionic strength increases. The second pathway is induced by stirring stress, yielding similar aggregation profiles irrespective of the starting condition.

Results

mAb1 opalescence and liquid-liquid phase separation are modulated by ionic strength

We first investigated the phase behavior of mAb1 as a function of ionic strength at RT in a relevant formulation buffer consisting of 10 mM histidine at pH 6.5. To achieve this, fresh solutions of mAb1 were prepared at a fixed concentration of 45 mg/mL and the ionic strength was varied through the addition of NaCl. Inspection of the resulting solutions revealed a non-linear relationship between the NaCl concentration and resulting opalescence/turbidity (Figure 1A). With increasing ionic strength, a high initial degree of opalescence was rapidly observed in the titration, followed by a subsequent decrease at higher salt concentrations. These observations were confirmed by the measurement of the light scattering intensity of the samples at a fixed angle (90°) (Figure 1B). To determine the origin of this high opalescence (which we will refer to as opalescence from now on), we next investigated selected mAb solutions by brightfield microscopy: the two extreme conditions of the NaCl titration series (0 and 150 mM NaCl, blue and green in Figure 1B) and two conditions yielding comparably high scattering intensities (10 and 22.5 mM NaCl, pink and purple in Figure 1B). As shown in Figure 1C, microscopy images of the 0 mM sample showed no clear indications of mesoscale self-association, whereas at 10 mM NaCl, highly dynamic droplets could easily be visualized, which readily coalesced upon contact and 'wetted' the glass surface of the microscopy slide within seconds, emphasizing their liquid-like nature (Figure S1). However, at 22.5 mM NaCl, no droplets or other assemblies resolvable by this technique were detected, in line with the early observation that conditions without any apparent large-scale association also give rise to a high degree of opalescence (18). Finally, increasing the NaCl concentration to 150 mM yielded a clear sample, similar to the 0 mM NaCl condition.

The presence of both opalescence as a single phenomenon or associated with LLPS in a narrow NaCl range complicates the determination of the LLPS regime by traditional techniques (e.g.

measurements of turbidity by light scattering). We therefore mapped the phase space over a broad range of mAb1 concentrations as a function of low NaCl concentrations where we observed the largest effect, using a high-throughput combinatorial microfluidic-based technique termed PhaseScan (45). Briefly, this method relies on the precise encapsulation of predefined combinations of mAb1, buffer (10 mM histidine pH 6.5) and NaCl solutions into microenvironments surrounded by an oil phase, for which the presence of droplets is individually assessed via fluorescence detection. As depicted in Figure 1D (and Figure S2), below 5 mM NaCl, no LLPS was detected at any mAb1 concentrations. By adding as little as 5 mM NaCl, LLPS was induced at mAb1 concentrations above an approximate apparent saturation concentration of 30 mg/mL. Remarkably, above 10 mM NaCl, the system returned to its original state i.e. underwent reentrant phase transition (46–50). Moreover, for most instances of detected LLPS, a large fraction of the droplets volume consisted of amorphous dense phase with high translational dynamics, readily adopting new shapes (Figure S3). From these results we can conclude that, under formulation relevant conditions, mAb1 depicts a complex phase behavior, displaying reentrant phase transition in a narrow NaCl range. Meanwhile, on the border of the LLPS spinodal line, opalescence is observed, yielding high light scattering intensities, not caused by the presence of well-defined dense droplets.

LLPS is driven by attractive interactions on the sub second timescale which are inhibited by L-arginine HCl

Based on the observations above, we further studied the protein-protein interactions underpinning mAb1 LLPS and opalescence by measuring small-angle X-ray scattering (SAXS) on our selected formulations at 45 mg/mL (Figure 2A). At high concentrations, the distances between mAb molecules and intramolecular distances reach similar orders of magnitude as a result of their dense packing, leading to a measurable distortion of the scattering signal I(**q**) of the mAb alone. This interparticle contribution, termed structure factor S(**q**), is primarily visible at small scattering angles (i.e. low **q**) in the absence of structural reorganization and reports on the presence of attractive (S(**q**)>1) or repulsive (S(**q**)<1) interactions, which we are interested in here. The structure factor contribution was obtained by dividing the total scattering intensity by that of a dilute mAb1 sample devoid of interparticle interactions (form factor) using on-line SEC-SAXS (Figure S4). By fitting the Guinier region (51) of the obtained form factor, we determined the radius of gyration of mAb1 to be 50 Å, as expected for a standard monoclonal antibody (Figure S4D) (52). As shown in Figure 2A, the structure factors for the LLPS (10 mM NaCl) and opalescent (22.5 mM NaCl) conditions had a similar shape, displaying highly attractive interactions, as inferred from the linear increase of structure factor at low **q**. Interestingly, positional correlation peaks were observed at **q**=0.06 $Å^{-1}$ and 0.1-0.12 $Å^{-1}$,corresponding to real space distances of 104 and 52 Å respectively, roughly equal to the diameter and radius of mAb1. This is in line with the S(**q**) data reported for other mAbs and points toward the formation of small equilibrium clusters in solution (6, 13, 53, 54). Altogether, this suggests that both LLPS and opalescence have the same underlying molecular grammar, and that these phenomena therefore can be mitigated using a similar approach. A common strategy to minimize LLPS/opalescence in mAb formulations relies on the addition of L-arginine HCl (10, 55). Indeed, adding 150 mM L-arginine HCl to a formulation in which mAb1 would have otherwise undergone LLPS (10 mM histidine pH 6.5 + 10 mM NaCl) no LLPS was observed, suggesting an inhibitory effect of L-arginine HCl on mAb1 LLPS (Figure S5). We further studied the extent of the inhibition of attractive interactions by L-arginine HCl and compared it to increasing the NaCl concentration to 150 mM, which similarly decreased the scattering and visual opalescence considerably (Figure 1). As shown in Figure 2A, a drastic reduction in the S(**q**) was observed for both conditions, albeit to a lower extent for the 150 mM NaCl condition, for which attractive interactions could still be observed compared to the sample containing L-arginine HCl, in which their formation is completely inhibited. Interestingly, the positional correlations mentioned above were also visible

for these two conditions but with decreased peak definition, probably due to the stronger screening of electrostatic interactions at higher ionic strengths (56).

Complementary insights into the in-situ phase separation of mAb1 were obtained through time-resolved SAXS measurements (TR-SAXS), by coupling a microfluidic device to the experimental setup at the beamline. In this sample environment, the laminar flow in the channels hydrodynamically focuses their constituent components, which passively diffuse to a junction point where they are mixed. The temporal resolution is then achieved by measuring SAXS at different distances from the mixing point on the chip, i.e. depending on the flowrate, each point on the z axis relates to a specific timepoint after mixing (Figure 2B). This approach enables the investigation of initial stages of LLPS, offering insights into the characteristics and progression of protein-protein interactions associated with this phenomenon over millisecond to second timescales. TR-SAXS experiments were performed by mixing mAb1 in 10 mM histidine pH 6.5 buffer with the same buffer supplied with NaCl to reach the final desired concentrations. Under LLPS inducing conditions, mAb1 interactions are already highly attractive 12 ms from the mixing point and remain so throughout the studied time range, demonstrating the rapid nature of the interactions conducive to LLPS (Figure 2C). This is also highlighted in Figure 2F where the average of the first three S(**q**) values at each timepoint of the individual conditions are summarized for a clearer overview of their temporal evolution. At 10 mM NaCl, the magnitude of the structure factor increases rapidly before fluctuating around a high mean value. When inhibiting the formation of dense phase by adding 150 mM L-arginine HCl, the S(**q**) measured at the first timepoint of 12 ms was considerably lower compared to the LLPS sample, switching from attractive to slightly repulsive interactions at 2.4 s (Figure 2D). For the 150 mM NaCl condition, a relatively higher structure factor was observed at the last timepoint in the TR-SAXS experiment, suggesting a more efficient suppression of attractive interactions by L-arginine HCl compared to NaCl, considering the slower diffusion in the mixing channel of the former. In all cases, the scattering curves of the final timepoints in the time-resolved experiment overlapped with the static SAXS data, showing a high level of agreement between the two setups (Figure S6).

LLPS/opalescence and stress-induced aggregation of mAb1 are decoupled

As a final step in the present study, we subjected our mAb1 formulations to overnight vigorous stirring (18 hours at 1000 rpm, RT), to detect any effect(s) of LLPS and opalescence on the physical stability. As shown in Figures 3A and B, stirring mAb1 samples resulted in a flagrant turbidity increase in all formulations. We noted that the turbidity in the 0 mM NaCl condition was less pronounced compared to the other conditions and that the 10- and 22.5- mM NaCl samples had maintained a mild opalescent appearance throughout the experiment. Interestingly, in our case, L-arginine HCl did not protect against contact stirring despite its reported role as a suppressor of protein-surface interactions and aggregation (57). The visibly aggregated samples were centrifuged for 2 hours at approximately 21.000 *g* to separate the pellet from the supernatant. To our surprise, pellets comparable in size were observed in all five different formulation conditions. Moreover, this revealed that the 10- and 22.5-mM NaCl samples clearly stayed opalescent after stirring, and that the molecular arrangements responsible for these phenomena also could sediment to some extent, revealing the presence of a transparent top dilute phase as observed in the case of mAb network formation (58). This was also the case for the non-stirred samples (Figure 3B).

We next performed a qualitative assessment of the generated particles by brightfield microscopy and confirmed that aggregates were formed in all formulations and responsible for the observed pellet (Figure 3C). It was further observed that their apparent morphologies varied between formulations, with smaller particles being formed at 0 mM NaCl, relatively larger at 150 mM NaCl and 10 mM NaCl+150 mM L-arginine HCl, while large, aggregate agglomerates were observed at 10 and 22.5 mM NaCl. Strikingly, droplets were observed in the soluble fraction of the stirred 10

mM NaCl sample, demonstrating that LLPS persists after harsh stirring or is able to reform rapidly thereafter (Figure 3C, bottom). Finally, we calculated the monomer recovery in the different formulations by measuring the concentration in the dilute phase divided by the starting concentration for all samples. Here, we added L-arginine HCl directly to the samples, to avoid non-linear concentration effects from the LLPS/opalescence. Within error, no differences in monomer recovery between the samples were detected, suggesting that the stirring-induced aggregation observed is independent of ionic strength (Figure 3E). Aggregation was observed even after the formulations were supplied with 0.15 mg/mL polysorbate 80 indicating that the observed effect described above does not solely arise from the air-water interphase but also from the bulk solution (Figure S7).

Discussion

In this work we explored the phase behavior of a model therapeutic mAb as a function of formulation-relevant parameters. Specifically, we evaluated the effect of ionic strength over a large drug product relevant concentration range (≈5-70 mg/mL) using a high-throughput combinatorial microfluidic droplet setup (PhaseScan) minimizing time and material requirements (Figure 1D). From this technique, we could rapidly deduce that mAb1 displayed reentrant phase separation, undergoing LLPS at RT, above a critical saturation concentration of 30 mg/mL and in an apparent NaCl range of ≈5-10 mM, after which it returned to its original mixed state, passing through an intermediate, highly opalescent LLPS-free phase. Interestingly, the scattering intensities were not symmetric around the phase border, with higher light scattering intensities measured above the upper critical NaCl concentration compared to the lower boundary, which could be explained by different molecular orientations in solution. Recently, reentrant phase behavior as a function of NaCl was reported for the intrinsically disordered Rabies Virus Phosphoprotein (RABV P) (59). Together with our present study on the multidomain mAb1, these represent two of the few studies showing that monovalent ions can induce reentrant phase transitions in protein systems.

The ability of mAb1 to phase separate at ambient temperature and with a relatively low saturation concentration is uncommon for mAbs. However, a similar case was reported for another mAb, mAb-B, and attributed to a strong enthalpic contribution capable of overcoming the entropic penalty of de-mixing and requiring high temperatures to shift the system toward a homogenously mixed state (60). The sharp response in phase behavior to a slight change in ionic strength suggests that electrostatic interactions are the main drivers of mAb1 LLPS. It is worth mentioning that from the above-mentioned setup alone, we cannot exclude that NaCl partitions into the phase-separated droplets and thereby influences the LLPS thermodynamics. Nevertheless, it can be speculated that in the region below the lower critical NaCl concentration, long-range repulsion is partially screened, enabling attractive short-range interactions, but not to an extent that is conducive to LLPS. Adding a small amount of NaCl might then further screen the long-range Coulomb repulsion between the mAb1 molecules and favor the association through short-ranged interactions into long-range networks leading to LLPS (21). In the vicinity of the upper critical NaCl concentration for LLPS of 10 mM NaCl, samples did not show signs of large-scale self-association but displayed high scattering/opalescence comparable to that of the LLPS region as exemplified here through the 22.5 mM NaCl condition, whose scattering and visual properties are indistinguishable from the phase-separated 10 mM NaCl condition, but is devoid of LLPS (Figure 1). This observation corroborates the relationship between opalescence and proximity to the critical region for LLPS (61, 62). Sequential additions of NaCl up to physiological concentrations decreased the level of self-assembly and returned the scattering intensity to roughly its original value, which is counterintuitive as the association is expected to increase as a result of the reduced Debye length (63). This peculiarity has been observed for several mAbs (6, 25, 29, 31) and has been attributed to the presence of electrostatically complementary patches on their surface (6). Used here as orthogonal techniques to the microfluidic approach mentioned above, quantification of the relative light scattering intensity at 90° as a function of NaCl in conjunction

with optical microscopy confirmed the lower NaCl boundary for LLPS. However, collecting more data above the apparent upper critical NaCl concentration for LLPS determined with the combinatorial microfluidic mixing revealed that it extended up to roughly 20 mM for our static concentration of 45 mg/mL mAb1 (Figure S7). In conclusion, the relationship between mAb concentration, ionic strength and self-assembly behavior can be highly non-linear and difficult to extrapolate to other mAb systems (64). However, techniques such as the microfluidic PhaseScan setup used here, capable of accessing a wide range of the design space integrated with complementary methods such as light scattering allow us to rapidly and sensitively tell two macroscopic manifestations of mAb self-assembly and potential developability issues apart: namely LLPS and high opalescence.

In a formulation development context, the characterization of physical stability phenomena linked to compromised product integrity is crucial to derive tailored mitigation strategies. However, most biophysical techniques require extensive sample dilution prior to analysis, drastically altering the physicochemical environment and interaction thermodynamics (65). To circumvent this, we applied SAXS to provide a quantitative characterization of the interactions involved in LLPS and opalescence at relevant concentrations. Reports of SAXS used in therapeutic mAb formulation development are scarce, compared to e.g. dynamic light scattering. However, this highly sensitive technique offers the advantage of simultaneously reporting on both colloidal and conformational stabilities and allows for high concentration studies (6, 13, 66, 67). Despite having clearly distinguishable features when studied by brightfield microscopy, the static SAXS curves for the LLPS and opalescent conditions were highly similar and characterized by the presence of small clusters known to arise from a combination of soft long-range electrostatic repulsion and short-range attraction at low ionic strength (6, 53, 54). This suggests that both phenomena rely on attractive interactions leading to cluster formation but that the small difference in ionic strength (10 vs 22.5 mM NaCl) dictates whether they will successfully assemble into a network capable of large-scale de-mixing or not. This is in line with observations for other mAb systems showing that increasing the ionic strength disrupts LLPS (25). When evaluated for the LLPS condition, addition of 150 mM L-arginine HCl led to a higher degree of inhibition of these interactions compared to increasing the NaCl concentration to 150 mM NaCl. This indicates that the effect of adding L-arginine HCl is not purely ionic since we observe a difference between the two samples, which have comparable ionic strengths. Interestingly, despite minimizing the degree of attractive interactions, the faint correlation peaks for clusters were still visible at these conditions, suggesting they might still be present but in very low amounts. In this study, we also applied SAXS coupled to a microfluidic mixing setup to achieve high control of the sample environment and add a temporal dimension to the analysis. This provides a quantitative characterization of the interactions involved in the onset and early stages of dynamic processes such as LLPS. In this time-resolved SAXS setup, the mixing is diffusion-driven, meaning that the relatively slower migration speed of large mAb1 molecules compared to the small ionic NaCl and buffer compounds will inevitably generate an inhomogeneous sample environment within the mixing channel and complicate the discrimination between dilution effects and actual structural rearrangements (68). Based on this, we rationalized the profile for the structure factor evolution in our LLPS condition in Figure 2F (pink trace) as follows: at first the mAb1 stock is slowly mixed with the buffer+NaCl stock solution, thereby approaching the phase border and leading to increasingly attractive interactions in solution until LLPS is formed, after which the S(**q**) stabilizes and remains unchanged.

In summary, mAb1 displays a peculiar phase behavior characterized by a reentrant phase transition within a narrow salt range. Just like our LLPS condition (10 mM NaCl), the selected condition (22.5 mM NaCl) directly flanking the upper critical NaCl concentration for LLPS is characterized by attractive interactions, the presence of small clusters and a high degree of opalescence, apparently only differing in the absence of droplets. This implies that the two phenomena are molecularly distinct and in the case of LLPS, mAbs can assemble into phase-separating networks when the correct balance of long-range repulsion and short-range attraction

is met. However, a small variation in ionic strength can result in a change in molecular attributes, resulting in the abrogation of LLPS and conservation of opalescence. SAXS analyses further reveal that the interactions underlying the LLPS phenomenon occur on the sub second timescale in solution, which can be specifically inhibited by L-arginine HCl. This technique is also able to detect potentially problematic residual attractive interactions in a visibly clear sample, which may guide formulation studies in saving time and valuable resources.

Finally, an important aspect of the fundamental study of therapeutic mAb self-association from a drug development perspective is to link this information to possible repercussions on the physical stability of the formulations (69). In practice, such studies are laborious and demand substantial resources (70). Stability studies are therefore complemented by forced degradation studies to generate a rapid proxy overview of the degradation profile of a drug product (71). This is usually achieved by subjecting mAb formulations to higher temperatures, shaking, freeze-thaw cycles, stirring and/or other stress factors (72). For mAbs, stirring represents one of the harshest physical perturbations and has been shown to rapidly induce the formation of large amounts of aggregates (73–76). The enhanced destabilizing effect of stirring has been explained by a mechanism in which the generation of conformationally altered mAbs adsorbed to the solid surface of the container can be recycled into the bulk solution through abrasion via contact with the stirring bar (75). In our forced degradation setup, stirring of all formulations produced solid pellets of comparable sizes, suggesting that its effect is independent of ionic strength in the timeframe studied. Importantly, LLPS was conserved for the 10 mM NaCl condition, coexisting with solid aggregates, while the opalescent sample (22.5mM NaCl) only displayed the latter, demonstrating that the two phenomena have distinct physical stability profiles. This was also the case for samples containing PS80, suggesting that the bulk solution also contributes to the overall aggregation, which is in line with the adsorption/abrasion mechanism described above (Figure S7). The fact that hard centrifugation wasn't enough to completely sediment LLPS droplets in the 10 mM NaCl sample suggests that their volume fraction is small and that there could exist an equilibrium between them and free, smaller clusters in solution. Finally, the observation that LLPS and opalescence were unaffected by stirring and that the same amount of mAb material was converted into aggregates in all formulation points toward the presence of two decoupled mechanisms. One in which mAb1 self-association is dependent on ionic strength, leading to cluster formation capable of undergoing LLPS under favorable conditions or remaining dispersed in solution and result only in opalescence. The other stress-induced mechanism is independent of ionic strength and hence LLPS/opalescence, resulting in the formation of solid aggregates (Figure 4). Traditionally, LLPS and opalescence have been viewed as precursors of aggregation in mAb formulations. Here, we report a not so straightforward relation between these phenomena, which should be taken into consideration during the rational design of mAb formulations. Taken together, our data demonstrate that mAbs can have a strikingly sensitive response to formulation parameters, displaying delicate zones of LLPS that are likely to be overlooked. We speculate that it might be possible to always identify excipient and mAb concentration combinations where LLPS can be brought to light, as long as one just searches carefully enough.

Materials and Methods

Model antibody

The model therapeutic mAb used in this work, mAb1, has a molecular weight ≈150 kDa and a pI ≈8, and was supplied by Novo Nordisk A/S in a proprietary formulation before being stored at -20°C as aliquots.

Buffer and stock preparation

A minimalistic buffer containing 10 mM L-histidine was prepared freshly using reagent grade L-histidine (ReagentPlus®, ≥99% TLC, H8000, Sigma Aldrich) in Milli-Q water with a specific

resistance of 18.2 MΩ/cm at 25°C. The buffering agent was allowed to dissolve on a magnetic stirrer before the pH was adjusted to pH 6.5 (+/- 0.05) using 1N Hydrochloric acid solution (c(HCl) = 1 mol/l (1 N), Titripur®, reag. Ph. Eur., reag. USP, 1.09057,1000, Supelco). Sodium chloride (1.37017.5000, Merck) and L-arginine HCl (EMPROVE® EXPERT, Ph. Eur., ChP, JP, USP, 1.01587, Sigma Aldrich) and polysorbate 80 stocks (1.37171, high purity, EMPROVE® EXPERT, Ph. Eur., ChP, JP, NF, Sigma Aldrich) were prepared freshly in analysis buffer (10 mM L-histidine pH 6.5) and filtered through a 0.1 um Whatman Anotop filter (GE Healthcare, Cat no: 6809-2012) mounted on a silicone free luer lock syringe (Henke Sass Wolf, Henke Ject®, Cat no: 4050-X00V0) pre-washed according to a previous protocol (77).

Buffer exchange by dialysis

Dialysis was carried out using Slide-A-Lyzer™ cassettes (Catalog number: A52976, Merck, 20 kDa MWCO) in a 10 mM histidine buffer adjusted to pH 6.5. The cassettes were first hydrated in a separate beaker with Milli-Q water before use. The procedure was carried out twice for two hours at room temperature (22°C) and overnight (16 hours) at 4°C using fresh buffer with a volume 500 times larger than the sample volume at each step.

Sample preparation

All samples were prepared in 10 mM histidine pH 6.5, directly from the freshly dialyzed mAb1 stock. Fresh NaCl stocks were used to prepare the different conditions. A 40 mM NaCl stock in 10 mM histidine pH 6.5 was used to prepare samples containing 2.5-22.5 mM NaCl, while a 500 mM NaCl stock was used for samples containing higher salt.

Sample concentration determination

Protein concentrations were determined as independent duplicates by measuring the UV-Vis absorbance at 280 nm on a NanoDrop™ One C spectrophotometer. Serial 1:1 dilutions of the stock solution in buffer were prepared from a factor 2 to 64. The absorbance of each dilution was measured using a theoretical molar extinction coefficient at 280 nm and the molecular weight before being multiplied by the dilution factor.

Right-angle static light scattering

Static light scattering experiments were performed at 90° with a 635 nm semiconductor laser, using the manual mode interface of the Labbot spectrophotometer (ProbationLabs, Sweden). A total volume of 400 µl for each sample was transferred to a high precision quartz glass, 10x4 mm light pathlength cuvette (Catalog number:104F-10-40, Hellma Analytics, Germany). Measurements were performed on independent duplicate samples, at room temperature (22°C) that were filtered through a pre-washed 0.1 um Whatman Anotop filter (GE Healthcare, Cat no: 6809-2012) mounted on a silicone free 1 mL luer lock syringe (B. Braun, Injekt®-F Luer Solo, Cat no: 9166017V). As soon as the scattering signal stabilized, ten consecutive measurements were performed before being averaged. The data was normalized to the highest scattering intensity.

Brightfield microscopy

Brightfield microscopic images were acquired at room temperature (22°C) with a Zeiss Axioscope 5 equipped with an Axiocam 305 color camera, through a LD Plan-Neofluar 20x/0.4 objective and processed using ImageJ software (78).

Combinatorial microfluidic mixing (PhaseScan)

The phase space of mAb1 as a function of NaCl was mapped out at room tmeperature using PhaseScan, according to published procedures (21, 45, 79). Pre-defined combinations of Alexa647 N-hydroxy succinimidyl (NHS) ester labeled mAb1, 10 mM histidine buffer (pH 6.5) and a 40 mM NaCl stock containing Alexa488 dye were encapsulated in HFE-7500 oil (FluoroChem) supplied with 1.2% (w/V) fluorosurfactant, (RAN Biotechnologies) by flowing the latter into the microfluidic device at a constant flowrate. A total of 46581 individual droplets containing pre-defined aqueous components were evaluated for the presence of LLPS using an inverted fluorescence microscope (OpenFrame, Cairn Research, Faversham, UK) equipped with a camera (Kinetix, Photometrics, Tucson, AZ, USA), through a 20x objective. The fluorescence intensities in the separate channels were used to back calculate the mAb1 and NaCl concentrations for each droplet.

Synchrotron size-exclusion chromatography (SEC)-SAXS for form factor determination

SEC–SAXS experiments were performed at the P12 EMBL BioSAXS beamline, at PETRA III, EMBL Hamburg, operated at a fixed energy (10 keV, λ = 0.124 nm). The form factor was determined at room temperature by SEC-SAXS using a Superdex S200 column coupled to an Agilent 1260 Infinity Bio-Inert high performance liquid chromatography (HPLC) system with an in-built temperature-controlled auto-sampler. A total volume of 70 µL mAb1 solution at a concentration of 10 mg/mL in 10 mM histidine pH 6.5+150 mM NaCl was injected into the column. The same buffer was used as mobile phase, and the flowrate was set to 0.65 mL/min. SAXS data was collected for the whole column run. The resulting frames were processed using CHROMIXS from the ATSAS package (80).

Static SAXS

SAXS of mAb1 at 45 mg/mL in 10 mM histidine pH 6.5 containing 10, 22.5 and 150 mM NaCl or 10 mM NaCl+ 150 mM L-arginine HCl was collected at the P12 beamline (PETRA III, DESY synchrotron, Hamburg), following standard procedures and at room temperature. For each sample, a buffer-buffer-sample-buffer-buffer measurement strategy was employed, and 50 frames were measured before averaging and buffer subtraction. Finally, the buffer-subtracted curves were absolute scaled in ATSAS, using a water and empty capillary measurements performed under the same conditions.(81). The structure factor S(**q**) was obtained by dividing the scaled subtracted scattering curve with the form factor.

Time-resolved solution SAXS

Time-resolved solution small-angle X-ray scattering was collected at the CoSAXS beamline at the MAX IV Laboratory, using a microfluidic sample delivery system. A detailed description of the technical design can be found elsewhere (68). Briefly, the sample is constantly flowing through a T shaped microfluidic-chip, with three inlets (cyclo-olefin copolymer COC/TOPAS®, 300x400 µm cross-section, Microfluidic ChipShop). Two out the three available inlets on the microfluidic chip, contained a dilution of the freshly dialyzed mAb stock, while the last inlet in the middle position was supplied with either fresh buffer or freshly prepared excipient (NaCl and/or L-Arginine HCl) stocks. At the mixing point on the microfluidic chip, the mAb is diluted by a factor of 2/3 (i.e. 45 mg/mL) and the excipients, by a factor of 1/3. SAXS data was collected at two of the inlets prior to mixing, the mixing point and 21 positions from the mixing point at a total flowrate of 60 µL/min as the chip was translated along **z**. The time resolution of the experiment was determined by a combination of the flowrate and the distance at which SAXS was measured from the mixing point. SAXS data were recorded with an incident X-ray beam of wavelength $\lambda = 0.99$ Å, with a sample-to-detector (Eiger2 X 4m) distance of 3.5 m yielding a q-range of $0.004 < \mathbf{q} < 0.3$ Å^{-1}. For each sample, the background of each inlet was measured prior to replacing the contents of the inlet 1 and 3 with mAb solution. A total of 40 frames were recorded at each point for a total of 50 ms and averaged, provided that they were of sufficiently good quality before being buffer subtracted. The scattering curves were then absolute scaled using water and empty capillary measurements

performed under the same conditions as standards. All processing was performed using the Primus package in the ATSAS data analysis software (81) and the structure factors were calculated as described in the previous section.

Stirring stress protocol

Selected mAb formulations were prepared as 1 mL solutions of 45 mg/mL mAb1. For the stirring study, 1 mL samples were filtered through a pre-washed 0.1 um Whatman Anotop filter (GE Healthcare, Cat no: 6809-2012) mounted on a silicone free 1 mL luer lock syringe (B. Braun, Injekt®-F Luer Solo, Cat no: 9166017V). and two aliquots of 500 µL were filled into separate 4 mL glass screw vials (45X15 mm, MD Scientific, VF013-1545) with a 5x2 mm cylindrical PFTE-coated stirring bar (BOLA, C 350-03). The vials were capped (Thermo Scientific, B7815-13) and sealed (Parafilm) before being placed vertically on a magnetic stirring plate (IKA RO 15) and stirred at 1000 rpm overnight (18h). Aliquots of the samples before stirring were diluted 10 times in 150 mM L-arginine HCl in 10 mM histidine pH 6.5 and their concentration measured.

Monomer recovery after stirring

After stirring, 2M L-arginine HCl in 10 mM histidine pH 6.5 was added directly to the vials to reach a final concentration of 150 mM. The vials were gently swirled and 400 µL aliquots were transferred to microcentrifuge tubes before 2 hours centrifugation at approximately 21000 *g*. Aliquots of the sample supernatants after stirring and centrifugation were diluted 10 times in 150 mM L-arginine HCl in 10 mM histidine pH 6.5 and their concentration measured, before being divided by the initial sample concentration (see previous section) to obtain what we called the monomer recovery here.

Acknowledgments

The authors acknowledge Novo Nordisk A/S for project funding and providing mAb material. The authors are also grateful for the assistance provided by the laboratory technicians in the CMC Biophysical Analysis team, especially Anders Marott, Helle Holton, Sisse Lakner Schmidt and Michala Cronberg. Furthermore, the authors are grateful to the CMC Late Phase Drug Product Development team at Novo Nordisk A/S, especially Mathias Hartwig Bjerager, Dorthe Kot Engelund and Britt Petersson. Tobias Palle Holm from the R&ED department at Novo Nordisk A/S is thanked for granting access to the microscope used in this study. The authors also thank Gaetano Invernizzi for mediating the collaboration with the University of Cambridge and general input. Tomas Sneideris is thanked for helping with the analysis of PhaseScan data shown in Figure S2. Christian Buch Parsbæk and Marco Polimeni are also thanked for their comments to the experiments and research paper. V.F. I.B. and S.L. acknowledge the support from the VILLUM FONDEN by the Villum Young Investigator Grants “Protein superstructure as Smart Biomaterials (ProSmart)” 2018-2023 (project number: 19175) and “Protein Phase Separation and Solid Transition in Synthetic Cells (ProSeC) 2024-2027 (project number: 53132). V.F. I.B. and S.L. also acknowledge the Novo Nordisk Foundation (projects NNF20OC0065260 and NNF22OC0080141) for financial support. The authors acknowledge the use of the MAX IV Laboratory for time on the CoSAXS beamline under proposal number 20231488. Research conducted at MAX IV, a Swedish national user facility, was supported by the Swedish Research council under contract 20188-07152, the Swedish Governmental Agency for Innovation Systems under contract 2018-04969 and Formas under contract 2019-02496. The authors further acknowledge DESY research center (Hamburg, Germany), for the provision of experimental facilities and time at PETRA III using beamline P22 (proposals 1188 and 1279).

References

1. O. Leavy, Therapeutic antibodies: past, present and future. *Nat Rev Immunol* **10**, 297–297 (2010).

2. J. K. H. Liu, The history of monoclonal antibody development - Progress, remaining challenges and future innovations. *Ann. med. surg.* **3**, 113–116 (2014).

3. A. Mullard, FDA approves 100th monoclonal antibody product. *Nat Rev Drug Discov* **20**, 491–495 (2021).

4. S. Crescioli, *et al.*, Antibodies to watch in 2024. *MAbs* **16,** 1-35 (2024).

5. K. Strebhardt, A. Ullrich, Paul Ehrlich's magic bullet concept: 100 years of progress. *Nat Rev Cancer* **8**, 473–480 (2008).

6. N. Skar-Gislinge, F. Camerin, A. Stradner, E. Zaccarelli, P. Schurtenberger, Using Cluster Theory to Calculate the Experimental Structure Factors of Antibody Solutions. *Mol Pharm* **20**, 2738–2753 (2023).

7. J. S. Kingsbury, *et al.*, A single molecular descriptor to predict solution behavior of therapeutic antibodies. *Sci Adv* **6**, 1-11 (2020).

8. P. G. Desai, *et al.*, An Intercompany Perspective on Practical Experiences of Predicting, Optimizing and Analyzing High Concentration Biologic Therapeutic Formulations. *J Pharm Sci* **112**, 359–369 (2023).

9. C. Narasimhan, H. Mach, M. Shameem, High-dose Monoclonal Antibodies Via the Subcutaneous Route: Challenges and Technical solutions, an Industry Perspective. *Ther Deliv* **3**, 889–900 (2012).

10. R. G. Strickley, W. J. Lambert, A review of Formulations of Commercially Available Antibodies. *J Pharm Sci* **110**, 2590-2608 (2021).

11. H. Ausserwöger, *et al.*, Non-specificity as the sticky problem in therapeutic antibody development. *Nat Rev Chem* **6**, 844–861 (2022).

12. E. J. Yearley, *et al.*, Observation of Small Cluster Formation in Concentrated Monoclonal Antibody Solutions and Its Implications to Solution Viscosity. *Biophys J* **106**, 1763–1770 (2014).

13. A. A. Chowdhury, *et al.*, Characterizing Protein–Protein Interactions and Viscosity of a Monoclonal Antibody from Low to High Concentration Using Small-Angle X-ray Scattering and Molecular Dynamics Simulations. *Mol Pharm* **20**, 5563–5578 (2023).

14. Y. Nakauchi, *et al.*, Opalescence Arising from Network Assembly in Antibody Solution. *Mol Pharm* **19**, 1160–1167 (2022).

15. C. Ishimoto, T. Tanaka, Critical Behavior of a Binary Mixture of Protein and Salt Water. *Phys Rev Lett* **39**, 474–477 (1977).

16. S. Alberti, A. Gladfelter, T. Mittag, Considerations and Challenges in Studying Liquid-Liquid Phase Separation and Biomolecular Condensates. *Cell* **176**, 419–434 (2019).

17. S. K. Singh, *et al.*, An Industry Perspective on the Monitoring of Subvisible Particles as a Quality Attribute for Protein Therapeutics. *J Pharm Sci* **99**, 3302–3321 (2010).

18. M. Sukumar, B. L. Doyle, J. L. Combs, A. H. Pekar, Opalescent Appearance of an IgG1 Antibody at High Concentrations and Its Relationship to Noncovalent Association. *Pharm Res* **21**, 1087–1093 (2004).

19. A. S. Raut, D. S. Kalonia, Pharmaceutical Perspective on Opalescence and Liquid–Liquid Phase Separation in Protein Solutions. *Mol Pharm* **13**, 1431–1444 (2016).

20. C.-K. Chow, B. W. Allan, Q. Chai, S. Atwell, J. Lu, Therapeutic Antibody Engineering To Improve Viscosity and Phase Separation Guided by Crystal Structure. *Mol Pharm* **13**, 915–923 (2016).

21. H. Ausserwöger, *et al.*, Surface patches induce nonspecific binding and phase separation of antibodies. *Proc. Natl. Acad. Sci. USA*. **120** (2023).

22. J. A. Thomson, P. Schurtenberger, G. M. Thurston, G. B. Benedek, Binary liquid phase separation and critical phenomena in a protein/water solution. *Proc. Natl. Acad. Sci. USA*. **84**, 7079–7083 (1987).

23. B. D. Mason, J. Zhang-van Enk, L. Zhang, R. L. Remmele, J. Zhang, Liquid-Liquid Phase Separation of a Monoclonal Antibody and Nonmonotonic Influence of Hofmeister Anions. *Biophys J* **99**, 3792–3800 (2010).

24. K. Reiche, J. Hartl, A. Blume, P. Garidel, Liquid-liquid phase separation of a monoclonal antibody at low ionic strength: Influence of anion charge and concentration. *Biophys Chem* **220**, 7–19 (2017).

25. H. Nishi, *et al.*, Phase Separation of an IgG1 Antibody Solution under a Low Ionic Strength Condition. *Pharm Res* **27**, 1348–1360 (2010).

26. N. R. Larson, *et al.*, Conformational Changes and Drivers of Monoclonal Antibody Liquid-Liquid Phase Separation. *J Pharm Sci* **112**, 680–690 (2023).

27. Y. Nakauchi, *et al.*, Opalescence Arising from Network Assembly in Antibody Solution. *Mol Pharm* **19**, 1160–1167 (2022).

28. Y. Wang, A. Lomakin, R. F. Latypov, G. B. Benedek, Phase separation in solutions of monoclonal antibodies and the effect of human serum albumin *Proc. Natl. Acad. Sci. USA*. **108**, 16606–16611 (2011).

29. G. Wu, *et al.*, Elucidating the weak protein-protein interaction mechanisms behind the liquid-liquid phase separation of a mAb solution by different types of additives. *Eur. J. Pharm.* **120**, 1–8 (2017).

30. J. E. Bramham, S. A. Davies, A. Podmore, A. P. Golovanov, Stability of a high-concentration monoclonal antibody solution produced by liquid–liquid phase separation. *MAbs* **13**, e1940666 (7 pages) (2021).

31. A. S. Raut, D. S. Kalonia, Opalescence in Monoclonal Antibody Solutions and Its Correlation with Intermolecular Interactions in Dilute and Concentrated Solutions. *J Pharm Sci* **104**, 1263–1274 (2015).

32. T. Matsuoka, R. Miyauchi, N. Nagaoka, J. Hasegawa, Mitigation of liquid–liquid phase separation of a monoclonal antibody by mutations of negative charges on the Fab surface. *PLoS One* **15**, 1-15 (2020).

33. Y. Wang, *et al.*, Quantitative Evaluation of Colloidal Stability of Antibody Solutions using PEG-Induced Liquid–Liquid Phase Separation. *Mol Pharm* **11**, 1391–1402 (2014).

34. Z. Tian, F. Qian, Adenosine Triphosphate-Induced Rapid Liquid–Liquid Phase Separation of a Model IgG1 mAb. *Mol Pharm* **18**, 267–274 (2021).

35. C. P. Brangwynne, *et al.*, Germline P Granules Are Liquid Droplets That Localize by Controlled Dissolution/Condensation. *Science (1979)* **324**, 1729–1732 (2009).

36. S. Wegmann, *et al.*, Tau protein liquid–liquid phase separation can initiate tau aggregation. *EMBO J* **37,** 1-21 (2018).

37. M. Fukuyama, *et al.*, Detection of Fibril Nucleation in Micrometer-Sized Protein Condensates and Suppression of Sup35NM Fibril Nucleation by Liquid–Liquid Phase Separation. *Anal Chem* **95**, 9855–9862 (2023).

38. M. Linsenmeier, *et al.*, The interface of condensates of the hnRNPA1 low-complexity domain promotes formation of amyloid fibrils. *Nat Chem* **15**, 1340–1349 (2023).

39. S. Ray, *et al.*, Mass photometric detection and quantification of nanoscale α-synuclein phase separation. *Nat Chem* **15**, 1306–1316 (2023).

40. A. M. Küffner, *et al.*, Sequestration within biomolecular condensates inhibits Aβ-42 amyloid formation. *Chem Sci* **12**, 4373–4382 (2021).

41. T. Das, *et al.*, Tunable metastability of condensates reconciles their dual roles in amyloid fibril formation. *Mol Cell* (2025), in press. https://doi.org/10.1016/j.molcel.2025.05.011.

42. E. Pantuso, *et al.*, On the Aggregation and Nucleation Mechanism of the Monoclonal Antibody Anti-CD20 Near Liquid-Liquid Phase Separation (LLPS). *Sci Rep* **10**, 8902 (2020).

43. J. E. Bramham, S. A. Davies, A. Podmore, A. P. Golovanov, Stability of a high-concentration monoclonal antibody solution produced by liquid–liquid phase separation. *MAbs* **13** (2021).

44. D. C. Ripple, M. N. Dimitrova, Protein particles: What we know and what we do not know. *J Pharm Sci* **101**, 3568–3579 (2012).

45. W. E. Arter, *et al.*, Biomolecular condensate phase diagrams with a combinatorial microdroplet platform. *Nat Commun* **13**, 7845 (2022).

46. T. Narayanan, A. Kumar, Reentrant phase transitions in multicomponent liquid mixtures. *Phys Rep* **249**, 135–218 (1994).

47. P. Pullara, I. Alshareedah, P. R. Banerjee, Temperature-dependent reentrant phase transition of RNA–polycation mixtures. *Soft Matter* **18**, 1342–1349 (2022).

48. G. L. Dignon, W. Zheng, Y. C. Kim, J. Mittal, Temperature-Controlled Liquid–Liquid Phase Separation of Disordered Proteins. *ACS Cent Sci* **5**, 821–830 (2019).

49. G. Krainer, *et al.*, Reentrant liquid condensate phase of proteins is stabilized by hydrophobic and non-ionic interactions. *Nat Commun* **12**, 1085 (2021).

50. H. Ausserwöger, *et al.*, Quantifying collective interactions in biomolecular phase separation. bioRxiv [Preprint] (2023). https://doi.org/10.1101/2023.05.31.543137 (accessed 7 July 2025)

51. A. Guinier, G. Fournet, Small-Angle Scattering of X-rays, G.Fournet, Ed. (Wiley, 1955)

52. S. Saurabh, *et al.*, Understanding the Stabilizing Effect of Histidine on mAb Aggregation: A Molecular Dynamics Study. *Mol Pharm* **19**, 3288–3303 (2022).

53. A. Stradner, *et al.*, Equilibrium cluster formation in concentrated protein solutions and colloids. *Nature* **432**, 492–495 (2004).

54. F. Cardinaux, *et al.*, Cluster-Driven Dynamical Arrest in Concentrated Lysozyme Solutions. *J Phys Chem B* **115**, 7227–7237 (2011).

55. S. Oki, S. Nishinami, Y. Nakauchi, T. Ogura, K. Shiraki, Arginine and its Derivatives Suppress the Opalescence of an Antibody Solution. *J Pharm Sci* **111**, 1126–1132 (2022).

56. A. Gulotta, *et al.*, Combining Scattering Experiments and Colloid Theory to Characterize Charge Effects in Concentrated Antibody Solutions. *Mol Pharm* **21**, 2250–2271 (2024).

57. S. Ren, Effects of arginine in therapeutic protein formulations: a decade review and perspectives. *Antib Ther* **6**, 265–276 (2023).

58. Y. Nakauchi, *et al.*, Opalescence Arising from Network Assembly in Antibody Solution. *Mol Pharm* **19**, 1160–1167 (2022).

59. F. Bouchama, *et al.*, Rabies Virus Phosphoprotein Exhibits Thermoresponsive Phase Separation with a Lower Critical Solution Temperature. *J Mol Biol* **437**, 1-25 (2025).

60. D. D. Banks, J. F. Cordia, Suppression of Electrostatic Mediated Antibody Liquid–Liquid Phase Separation by Charged and Noncharged Preferentially Excluded Excipients. *Mol Pharm* **18**, 1285–1292 (2021).

61. E. S. R. Gopal, Critical opalescence. *Resonance* **5**, 37–45 (2000).

62. B. A. Salinas, *et al.*, Understanding and Modulating Opalescence and Viscosity in a Monoclonal Antibody Formulation. *J Pharm Sci* **99**, 82–93 (2010).

63. W. Li, *et al.*, Charge-Induced Patchy Attractions between Proteins. *J Phys Chem B* **119**, 503–508 (2015).

64. J. Zarzar, *et al.*, High concentration formulation developability approaches and considerations. *MAbs* **15** (2023).

65. P. Garidel, A. B. Kuhn, L. V. Schäfer, A. R. Karow-Zwick, M. Blech, High-concentration protein formulations: How high is high? *Eur. J. Pharm.* **119**, 353–360 (2017).

66. X. Tian, A. E. Langkilde, M. Thorolfsson, H. B. Rasmussen, B. Vestergaard, Small-Angle X-ray Scattering Screening Complements Conventional Biophysical Analysis: Comparative Structural and Biophysical Analysis of Monoclonal Antibodies IgG1, IgG2, and IgG4. *J Pharm Sci* **103**, 1701–1710 (2014).

67. W. D. Kimball, *et al.*, Growth of Clusters toward Liquid–Liquid Phase Separation of Monoclonal Antibodies as Characterized by Small-Angle X-ray Scattering and Molecular Dynamics Simulation. *J Phys Chem B* **129**, 2856–2871 (2025).

68. F. Herranz-Trillo, *et al.*, “Time-resolved scattering methods for biological samples at the CoSAXS beamline, MAX IV Laboratory” in *Methods Enzymol.*, P. Moody, H. Kwon, Eds. (2024), pp. 245–296.

69. H. Kaur, Stability testing in monoclonal antibodies. *Crit Rev Biotechnol* **41**, 692–714 (2021).

70. J. Wiesbauer, M. Cardinale, B. Nidetzky, Shaking and stirring: Comparison of controlled laboratory stress conditions applied to the human growth hormone. *Process Biochem.* **48**, 33–40 (2013).

71. A. Hawe, *et al.*, Forced Degradation of Therapeutic Proteins. *J Pharm Sci* **101**, 895–913 (2012).

72. C. Nowak, *et al.*, Forced degradation of recombinant monoclonal antibodies: A practical guide. *MAbs* **9**, 1217–1230 (2017).

73. T. Ishikawa, N. Kobayashi, C. Osawa, E. Sawa, K. Wakamatsu, Prevention of Stirring-Induced Microparticle Formation in Monoclonal Antibody Solutions. *Biol Pharm Bull* **33**, 1043–1046 (2010).

74. S. N. Telikepalli, *et al.*, Structural Characterization of IgG1 mAb Aggregates and Particles Generated Under Various Stress Conditions. *J Pharm Sci* **103**, 796–809 (2014).

75. A. S. Sediq, R. B. van Duijvenvoorde, W. Jiskoot, M. R. Nejadnik, No Touching! Abrasion of Adsorbed Protein Is the Root Cause of Subvisible Particle Formation During Stirring. *J Pharm Sci* **105**, 519–529 (2016).

76. S. Telikepalli, *et al.*, Physical Characterization and In Vitro Biological Impact of Highly Aggregated Antibodies Separated into Size-Enriched Populations by Fluorescence-Activated Cell Sorting. *J Pharm Sci* **104**, 1575–1591 (2015).

77. C. Thorlaksen, M. B. Neergaard, M. Groenning, V. Foderà, “Reproducible Formation of Insulin Superstructures: Amyloid-Like Fibrils, Spherulites, and Particulates” in *Methods Mol. Biol*, (Humana Press Inc., 2023), pp. 297–309.

78. C. A. Schneider, W. S. Rasband, K. W. Eliceiri, NIH Image to ImageJ: 25 years of image analysis. *Nat Methods* **9**, 671–675 (2012).

79. H. Ausserwöger, *et al.*, Biomolecular condensates sustain pH gradients at equilibrium through charge neutralisation. bioRxiv [Preprint] (2024). https://doi.org/10.1101/2024.05.23.595321 (accessed 7 July 2025).

80. A. Panjkovich, D. I. Svergun, CHROMIXS: automatic and interactive analysis of chromatography-coupled small-angle X-ray scattering data. *Bioinformatics* **34**, 1944–1946 (2018).

81. K. Manalastas-Cantos, *et al.*, *ATSAS 3.0* : expanded functionality and new tools for small-angle scattering data analysis. *J Appl Crystallogr* **54**, 343–355 (2021).

Figures

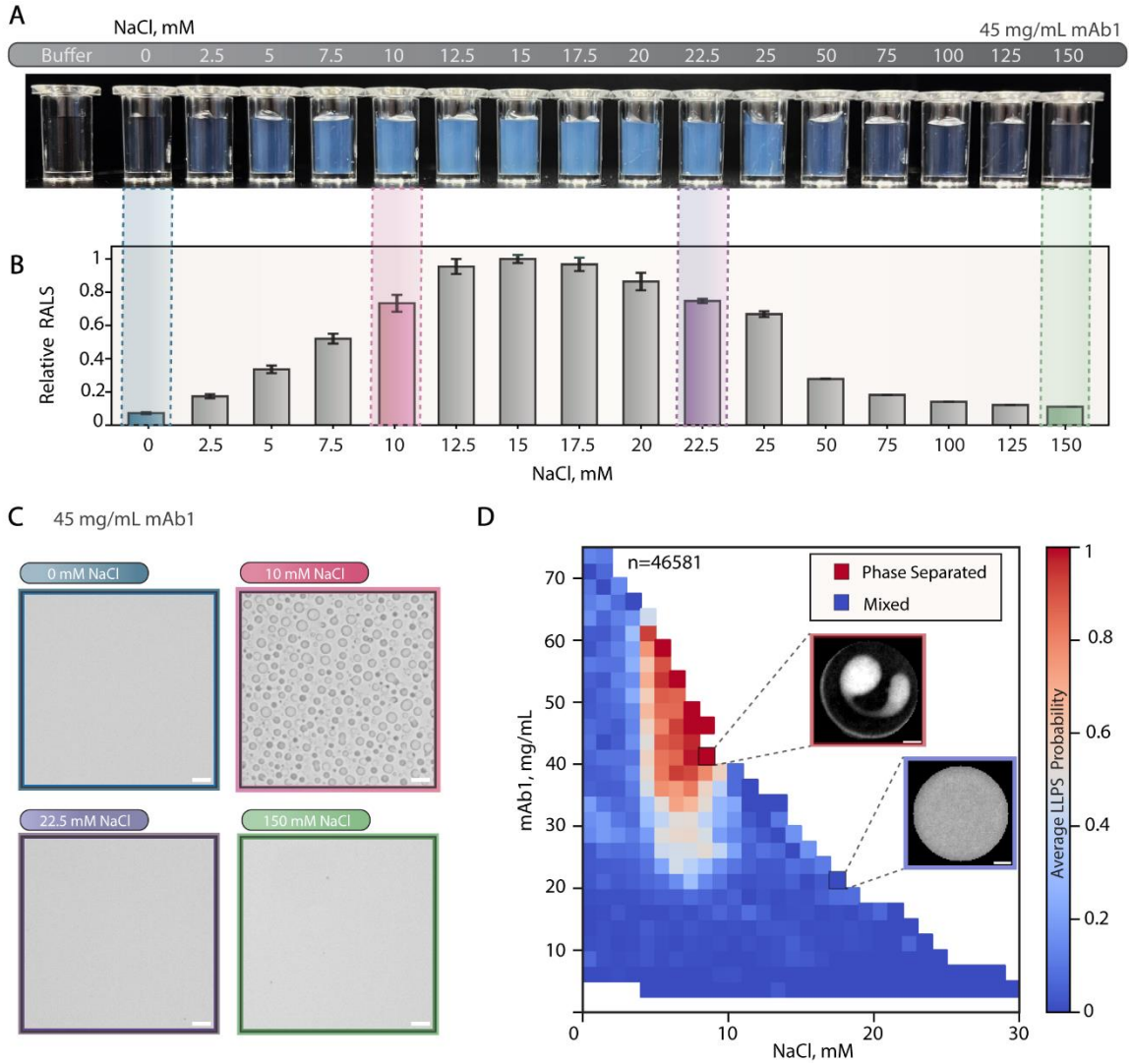

Figure 1. Phase behavior of mAb1 (A) Visual appearance and (B) normalized right-angle scattering intensities at 635 nm of 45 mg/mL mAb1 solutions as a function of NaCl (0-150 mM), where the NaCl concentrations selected for microscopy are highlighted in blue, pink, purple and green. The experiments were independently performed n=2 times and errors represent standard deviations of the duplicate measurements. (C) Brightfield microscopy images of selected conditions (0, 10, 22.5 and 150 mM NaCl, 20 µm scalebar). (D) Liquid-liquid coexistence curve of mAb1 versus NaCl concentration, evaluated by a combinatorial microfluidic mixing setup with fluorescence microscopy-based LLPS detection. The resulting grid-map was achieved by binning the n = 46581 individual data points (Figure S2) to evaluate the local average phase separation probability (LLPS probability = 1: red, 0.5: white, 0: blue), as described in (79). The insets with red and blue borders show representative microscopy images of phase-separated mAb1 inside the mAb1/buffer/NaCl in oil microemulsion droplets and one with no detected LLPS, respectively.

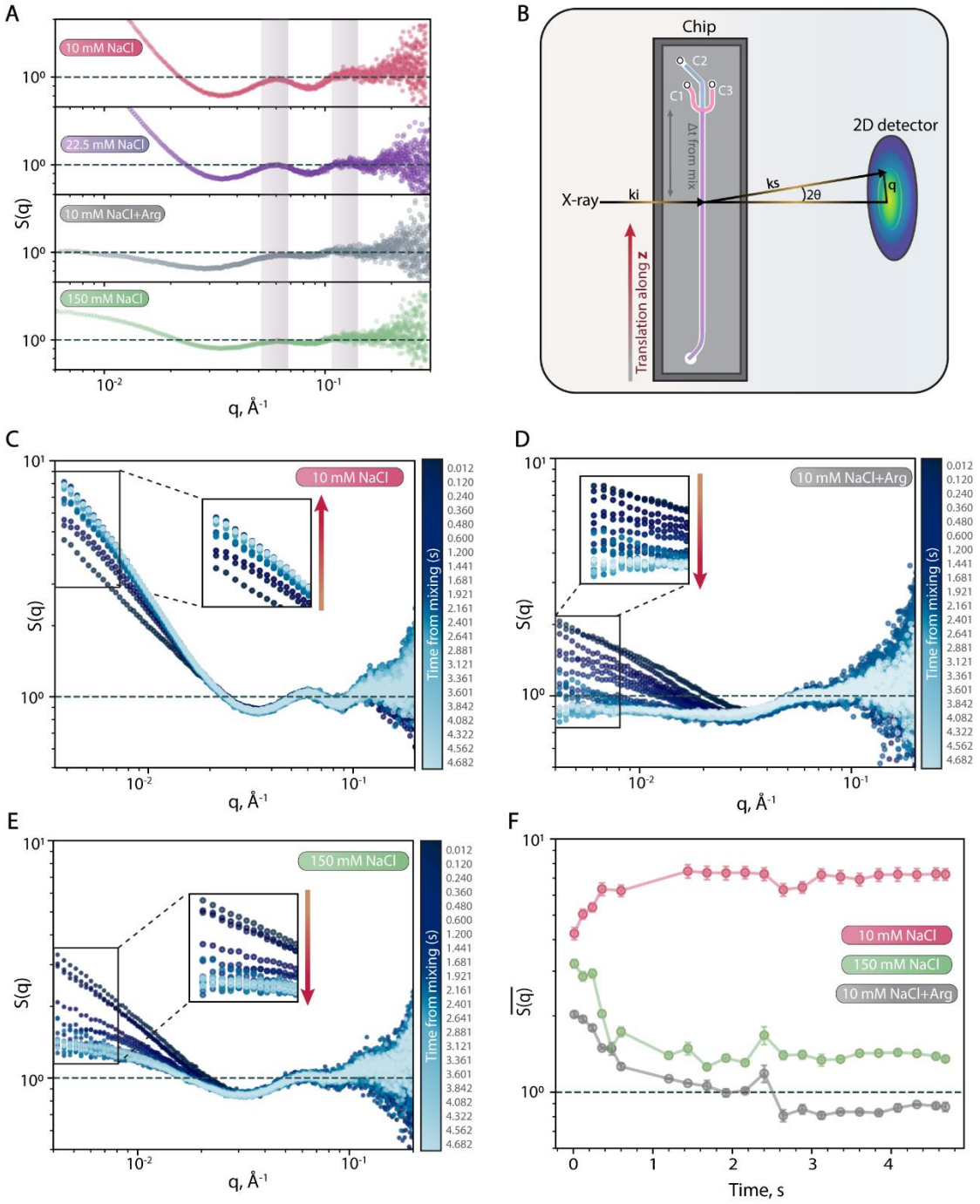

Figure 2. Characterization of interactions underlying mAb1 LLPS with SAXS (A) Structure factor measured for 45 mg/mL mAb1 + 10 mM NaCl, 22.5 mM NaCl, 10 mM NaCl + 150 L-arginine HCl (called 10 mM NaCl+Arg here) and 150 mM NaCl, from static SAXS experiments (B) Schematic representation of the microfluidic chip coupled to the Co-SAXS beamline. (C)-(E) Time-resolved SAXS data of 45 mg/mL + (C) 10 mM NaCl, (D) 10 mM NaCl + 150 mM L-arginine HCl and (E) 150 mM NaCl recorded at 22 distances from the mixing point across the channel. The distances were converted to timepoints here. Data was recorded at a total flowrate of 60

μL/min (F) Average and associated standard deviations of the first three S(**q**) values for each timepoint of the time-resolved SAXS data as a function of time from the mixing point.

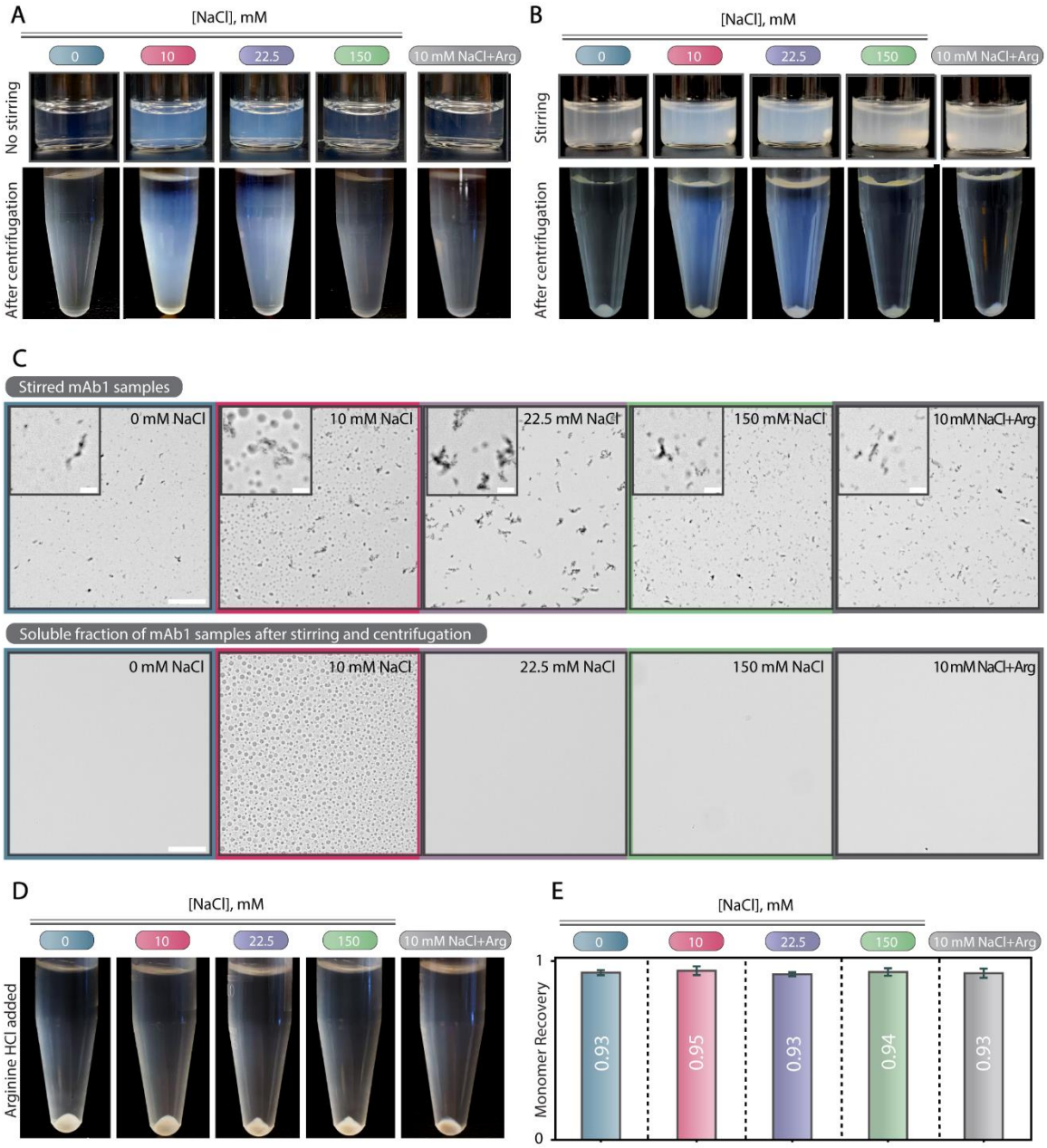

Figure 3. Physical stability of mAb1 samples as a result of stirring stress. Visual appearance of 45 mg/mL mAb1 solutions in 10 mM histidine pH 6.5 at 0, 10, 22.5, 150 mM NaCl or 10 mM NaCl+150 mM L-arginine HCl (10 mM NaCl+Arg) before (A) and after (B) magnetic stirring overnight (approximately 18 hours) at 1000 rpm and subsequent centrifugation at approximately 21000 *g* for 2 hours at RT. (C) Brightfield microscopy of the stirred samples and the supernatant after centrifugation (50 µm scalebar). (D) Representative images of the stirred and centrifuged samples with added L-arginine HCl. Samples were prepared at a larger volume for the images, for increased clarity (E) Monomer recovery of the different conditions, measured on two independent samples. The numbers on the individual bars represent the calculated monomer recovery, where 1 and 0 stand for complete and no monomer recovery, respectively. Errors represent standard deviations from duplicate measurements.

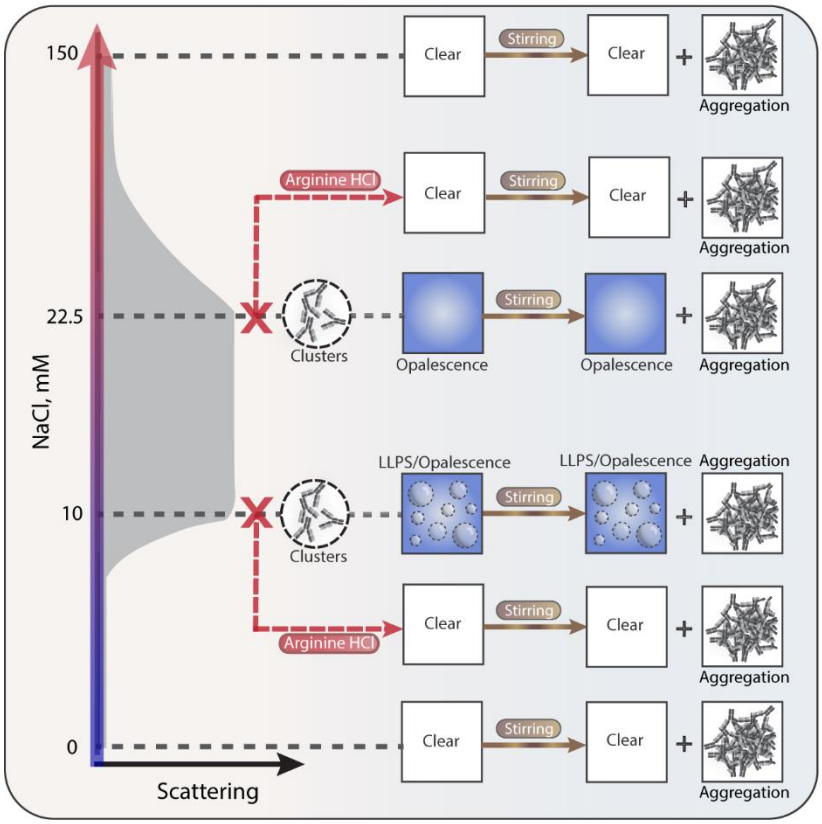

Figure 4: Summary of mAb self-assembly behavior at 45 mg/mL, as a function of NaCl concentration and applied stirring stress. mAb1 LLPS and opalescence occur in a narrow NaCl range and can be inhibited by L-arginine HCl. Solid aggregation is decoupled from LLPS and opalescence. LLPS and opalescence are unaffected by stirring induced stress.

Supporting Information for

Decoupling liquid-liquid phase separation and opalescence from stress-induced aggregation in therapeutic mAb formulations

Inna Brakti[a,b,1], Samuel Lenton[a,1], Hannes Ausserwöger[c], Rob Scrutton[c], Nikolai Lorenzen[d], Martin Nors Pedersen[b], Jesper Søndergaard Marino[e], Fátima Herranz-Trillo[f], Ann E. Terry[f], Tuomas P. J. Knowles[c], Minna Grønning Jensen[b], Vito Foderà[a]

[a]Department of Pharmacy, University of Copenhagen, Copenhagen, Denmark 2100, [b]Biophysical Analysis, CMC Analytical Support, Novo Nordisk A/S, Måløv, Denmark 2760, [c]Yusuf Hamied Department of Chemistry, Centre for Misfolding Diseases, University of Cambridge, Cambridge, United Kingdom CB2 1EW, [d]Biophysics and Injectable Formulation, Global Research Technologies, Novo Nordisk A/S, [e]Process Optimisation, Digital Science and Innovation, Novo Nordisk A/S, Måløv, Denmark 2760, Måløv, Denmark 2760,[g]MAX IV Laboratory, Lund University, Fotongatan 2, 224 84 Lund, Sweden

* Vito Foderà

Address: Department of Pharmacy, University of Copenhagen, Copenhagen, Denmark 2100

Phone: +4535336131

Email: vito.fodera@sund.ku.dk

*Minna Grønning Jensen

Address: Biophysical Analysis, CMC Analytical Support, Novo Nordisk A/S, Måløv, Denmark 2760

Phone: +4530753421

Email: mgqj@novonordisk.com

This file includes:

Figures S1 to S7

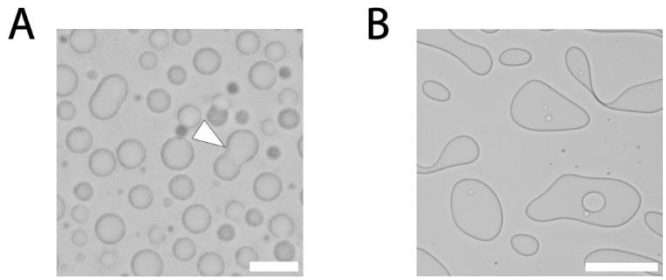

Figure S1: mAb1 LLPS is liquid-like (A) Coalescence of droplets, as indicated by the white arrowhead (10 µm scalebar). (B) Wetting of the glass surface of the microscopy slide over time (100 µm scalebar)

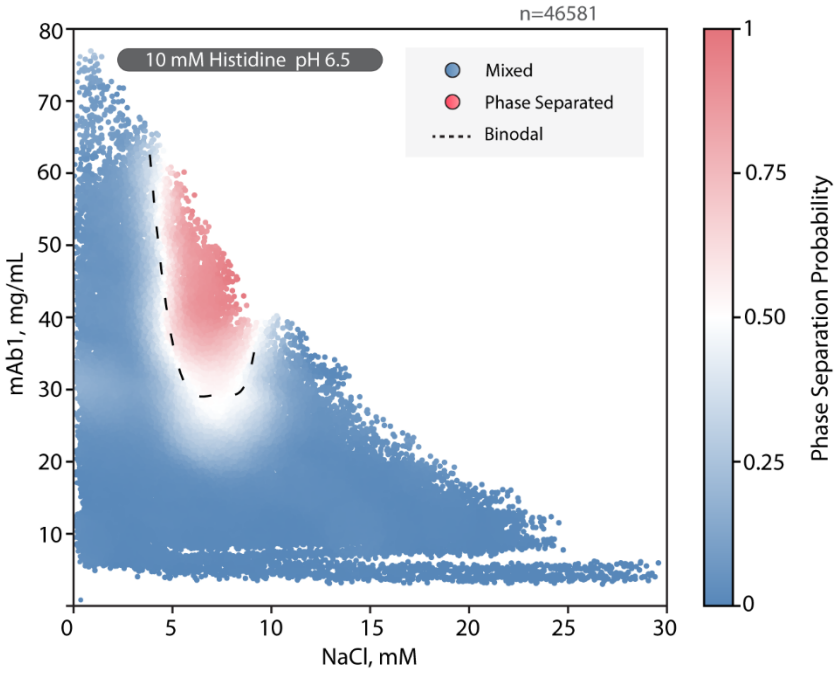

Figure S2: Coexistence curve of mAb1 as a function of NaCl determined using combinatorial microfluidics. Each of the 46581 observations is shaded according to phase separation probability based on local radial averaging. An eye guide for the approximate location of the binodal is indicated by the dashed black line.

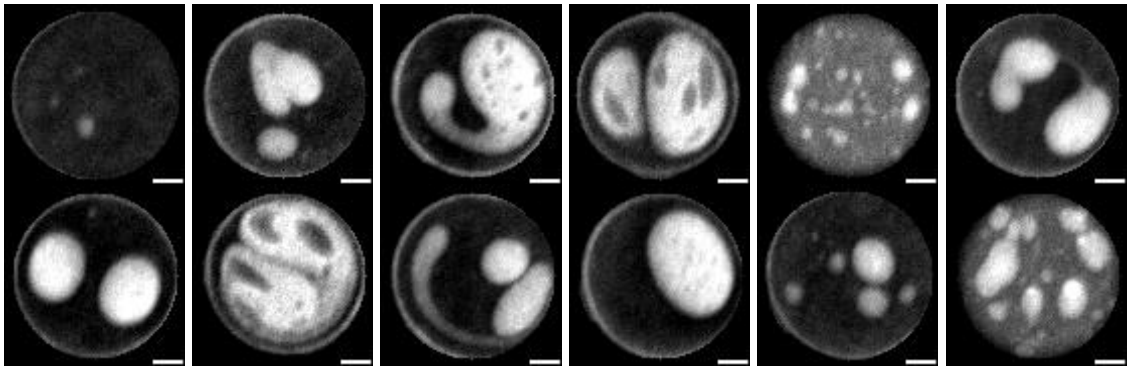

Figure S3: Selected dense phase morphologies detected with PhaseScan using fluorescence microscopy (20 µm scalebar)

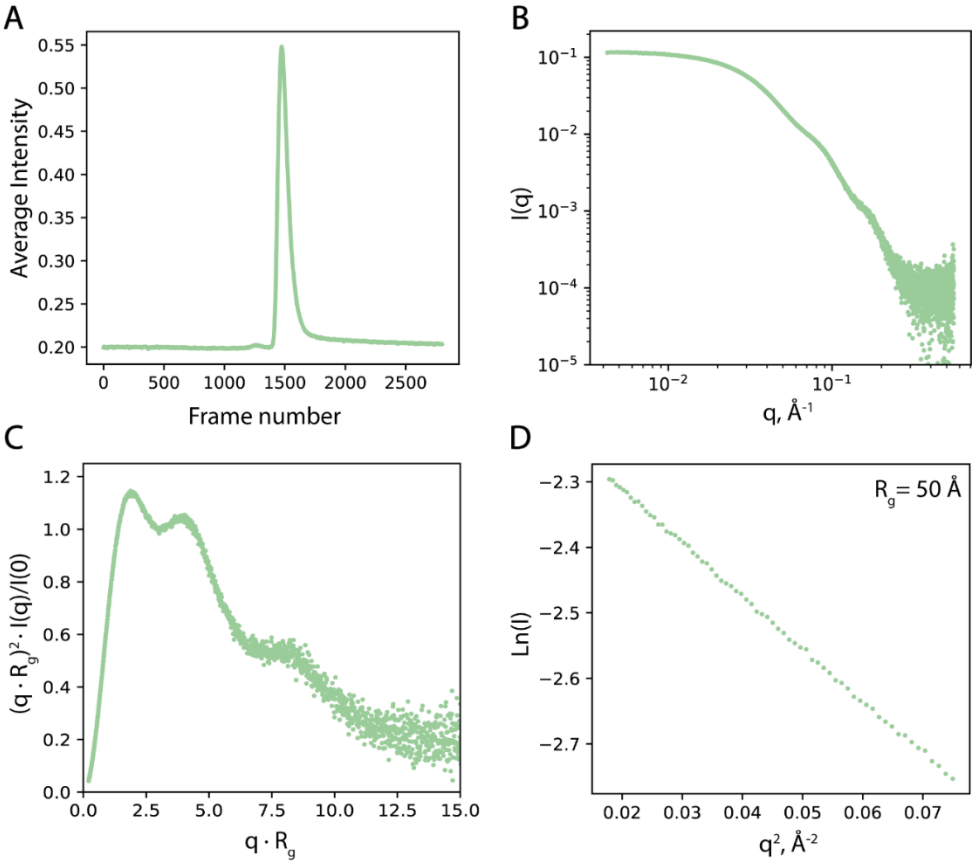

Figure S3: Overview of SEC SAXS measurements of mAb1 (A) Elution profile of 10 mg/mL mAb1 in 10 mM histidine pH 6.5 + 150 mM NaCl mobile phase showing the average integrated SAXS intensity I(q) ($1.48*10^{-3}$ $Å^{-1}$ < **q** < 0.556 $Å^{-1}$) as a function of frame number (B) Average scattering curve of frames **Figure S3 (continued):** 1454 to 1521, corresponding to monomeric mAb1 (highest peak of the elution profile in A) (C)

Dimensionless Kratky plot showing three peaks, as expected for IgG molecules (D) Guinier plot for the monodisperse mAb1 sample showing linearity in the Guinier range and the radius of gyration determined from the slope.

Figure S4: Suppression of LLPS and opalescence with L-arginine HCl and effect of stirring the latter (A) Visual appearance of an LLPS sample containing 45 mg/mL mAb1 in 10 mM histidine, 10 mM NaCl, pH 6.5 compared to 45 mg/mL mAb1 in 10 mM histidine, 10 mM NaCl, 150 mM L-arginine-HCl, pH 6.5 (10 mM NaCl+Arg). The latter was added prior to adding the NaCl that would have otherwise made the sample undergo LLPS (left) Brightfield microscopy of the 10 mM NaCl+Arg sample showing that no LLPS is detected under these conditions. The scalebar represents 50 µm. (B) Same setup as in (A) but with the 22.5 mM (opalescent sample) as well as images of the effect of stirring at 1000 rpm overnight (18 hours), showing the increased visual turbidity of the sample and the presence of aggregates in the microscopy image.

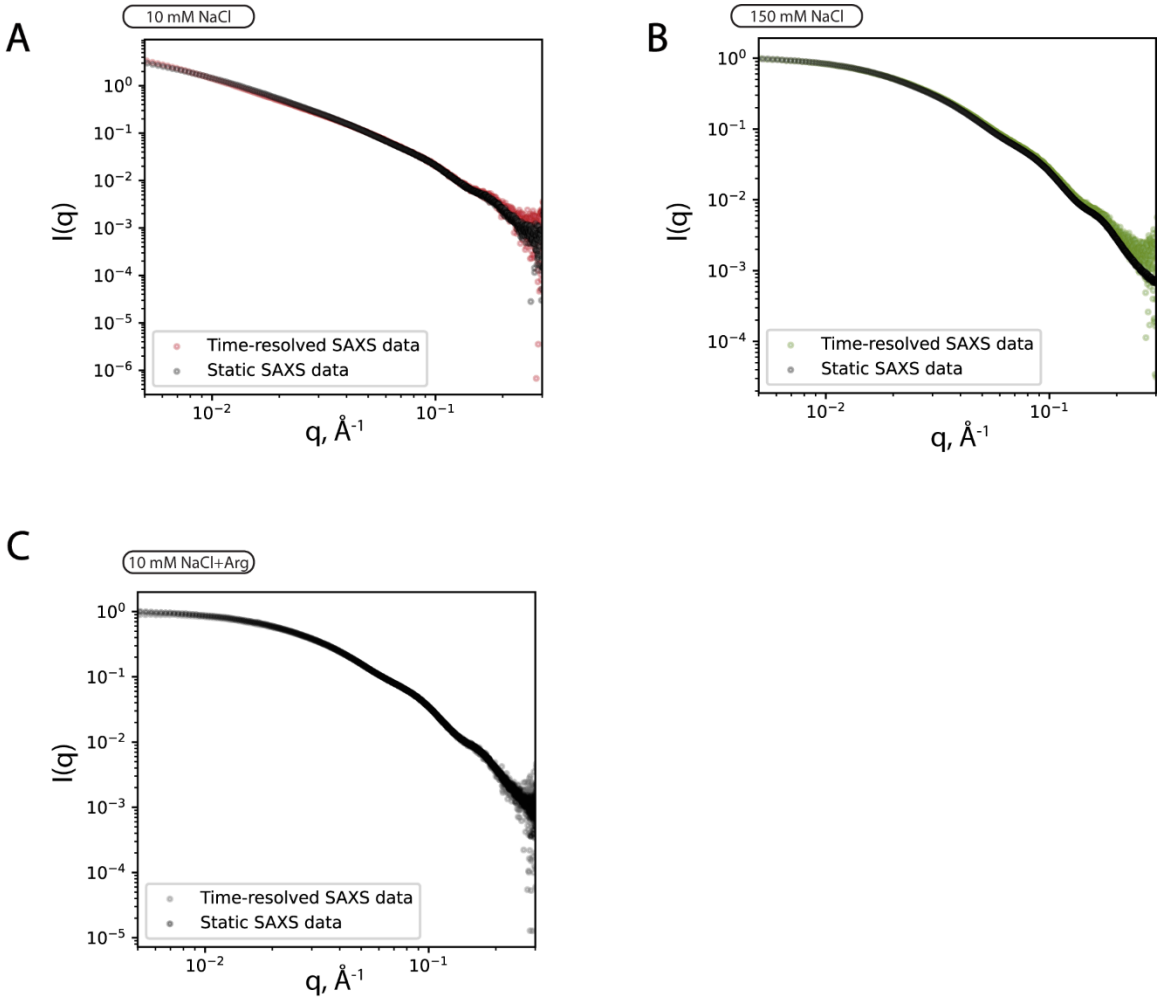

Figure S5: Overlay of the scattering curves (intensity I(q) vs q) for the last timepoint in the time resolved SAXS experiments (black curves) and scattering curves from the static SAXS experiment (colored curves) for 45 mg/mL mAb1 in 10 mM histidine pH 6.5 containing 10 mM NaCl (A), 150 mM NaCl (B) or 10 mM NaCl + 150 mM arginine HCl (C)

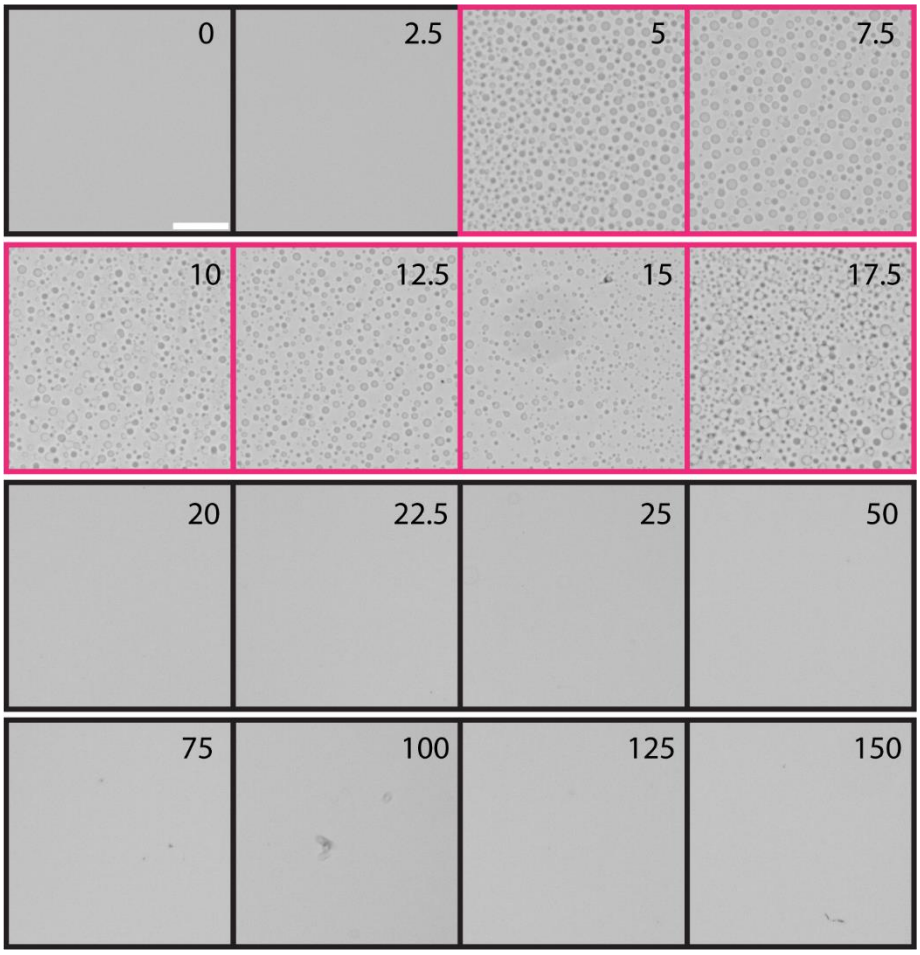

Figure S6: Phase boundary of mAb1 as a function of NaCl determined with optical microscopy. Brightfield microscopy of 45 mg/mL mAb1 in 10 mM histidine pH 6.5 at room temperature as a function of NaCl concentration (0, 2.5, 5, 7.5, 10, 12.5, 15, 17.5, 20, 22.5, 25, 50, 75, 100, 125, 150 mM) with LLPS region highlighted in pink. The scalebar represents 50 µm.

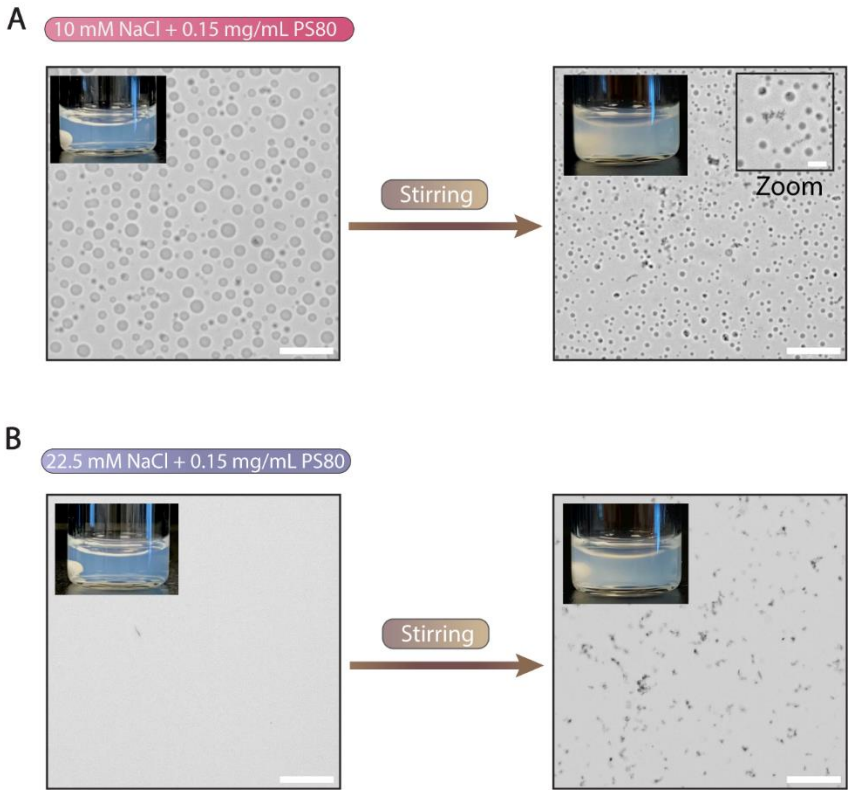

Figure S7: Effect of PS80 on the stirring induced aggregation (A) Visual appearance and brightfield microscopy images of 45 mg/mL mAb1 in 10 mM histidine pH 6.5 containing 10 (A) or 22.5 (B) mM NaCl with 0.15 mg/mL PS80 added. The left images are before stirring and the images on the right are after overnight stirring as described in the Materials and Methods section. The scalebar represents 50 µm in the main microscopy image and 10 µm in the inset zoom image. In the 10 mM NaCl + 0.15 mg/mL PS80 images, the difference in droplet size arises from their fast dynamics and difference in times at which the images were acquired.